# Multistability, nonlinear response and wave propagation in self-humidified PEM fuel cells

Y. De Decker [a],[*], J.B. Benziger [b],[**], E. Kimball [b], I.G. Kevrekidis [b]

[a] *Interdisciplinary Center for Nonlinear Phenomena and Complex Systems, Université Libre de Bruxelles, Campus Plaine, CP 231 bd du Triomphe, 1050 Brussels, Belgium*
[b] *Department of Chemical Engineering, Princeton University, Princeton, NJ 08544, USA*

## ARTICLE INFO

## ABSTRACT

A simple tanks-in-series model is presented, which allows for the understanding of the basic physics behind complex spatiotemporal behaviors observed in self-humidified polymer electrolyte membrane (PEM) fuel cells. Our approach is focused on how the intrinsically nonlinear dynamics of water formation couples with water transport, leading to multistability, inhomogeneous steady state current profiles through the cell and other nonlinear phenomena. We show in particular how the operating parameters determine the location of high current spots and the subsequent propagation of current waves throughout the cell during the ignition procedure. We also reproduce and explain transient current increases seen during the extinction of the cell and the unusual aspect of the polarization curves. Implications for the efficiency of self-humidified PEM fuel cells are highlighted, and possible ways to improve their performances are discussed on these bases.

## 1. Introduction

Fuel cells promise to be an efficient, realistic and reliable environment-friendly alternative to the traditional combustion engine (Martin, 2005; Fronk, 2005). The conversion of chemical into electrical energy in these devices does not suffer from the Carnot limitations associated with heat engines, so that fuel cells are typically capable of delivering energy with a high efficiency. Polymer electrolyte membrane (PEM) fuel cells, in which protons traverse a proton exchanging membrane separating the anode from the cathode, are seen as the most attractive solution for automotive transportation.

Fuel cells differ from the traditional batteries, in the sense that they are not closed systems but open ones, due to a constant exchange of reactants and products with the environment. They are, in effect, *chemical reactors* with the voltage associated with chemical potential difference across the electrolyte being the driving force for reaction, and the current being a measure of the reaction rate. Through the last several years we have been developing an experimental and theoretical program centered around a "reaction engineering" approach of simplified PEM fuel

cells based on the $H_2/O_2$ reaction. In the case of small self-humidified cells (dry feeds), which can be seen as stirred tank reactors (STRs), complex dynamical features were observed, including multistability, current ignition and extinction, etc. (Moxley et al., 2003; Chia et al., 2004). These phenomena could be traced back to the intrinsically autocatalytic character of such cells: water created by the reaction humidifies the PEM, which reduces its resistance with respect to proton conduction, which in turn increases the current flowing through the cell and hence the rate of $H_2O$ formation (Benziger et al., 2004, 2005). This is remarkably analogous to the positive feedback occurring for exothermic chemical reactions in a STR (Luss, 1997; Marwaha and Luss, 2003; Marwaha et al., 2004).

In this work we focus on *spatially extended* PEM fuel cells. Indeed, we recently developed a modified cell with a segmented anode, allowing for the real-time monitoring of the current as a function of the distance from the gas inlets. As was reported earlier (Benziger et al., 2007b), we observed a wave-like propagation of the current throughout these "plug-flow"-like cells which can be thought of as analogous to propagating flames observed in combustion processes. It should be emphasized that Nazarov and Promislow (2006) had at this time presented numerical simulations showing front propagation and associated long time constants on the basis of some of our previous results, i.e. before we reported the existence of such waves. The simulated temporal response of the current, however, strongly differed qualitatively from our observations, and the reasons behind this discrepancy

[*] Corresponding author.
[**] Principal corresponding author.
*E-mail addresses:* ydedecke@ulb.ac.be (Y. De Decker), benziger@princeton.edu (J.B. Benziger), ekimball@princeton.edu (E. Kimball), yannis@arnold.princeton.edu (I.G. Kevrekidis).

remain unclear. The complexity of this model also did not allow for a clear understanding of the main parameters governing the formation of these patterns. In order to clarify the origin of the observed waves, we proposed a simple, semi-quantitative model focusing on the basic physicochemical mechanism behind these phenomena (Benziger et al., 2007b). This study revealed the central role played by water formation and transport in the emergence and subsequent propagation of "wet spots" in the cell. Since then, more sophisticated models have been proposed for self-humidified PEM fuel cells (Hanke-Rauschenbach et al., 2008; Grötsch et al., 2008) but they mainly focus on current–voltage characteristics and bifurcation analysis of spatially lumped models.

In this work, we perform a systematic parametric study (bifurcation analysis) of our previously introduced, spatiotemporal model and compare the predictions made in different flow configurations with newly available experimental data on the shutdown dynamics and electrochemical properties of the cells (Benziger et al., 2007a). As will be shown, the simple model qualitatively reproduces the main features of the real system. The steady state global current and current profile through the cell, the spatiotemporal propagation of the reaction and the electrochemical properties of the cell (*i–V* curves) are predicted semi-quantitatively. Thanks to the simplicity of the model, an intuitive explanation can be given as to how and why the presence of current patterns could affect the efficiency and the dynamic response of self-humidified PEM fuel cells. We show in particular what parameters affect the time necessary to ignite or extinguish the cell, the location of current "hot spots" and their subsequent propagation. We also assess, on the basis of this model, the possibility to run the cell in "extreme" conditions, for example at relatively high temperatures.

The paper is organized as follows. We first briefly present the experimental setup allowing for the study of the spatiotemporal dynamics of our simplified PEM fuel cells. We then present and discuss the kinetic model that will form the theoretical basis of our investigation. In the following section we present the steady state properties of the model, along with the corresponding results from experiments. We also discuss the spatiotemporal behavior of the system under consideration, including the polarization curves (Section 5). In the last section, we discuss the potential implications of these specific kinetics for a fuel cell operating under realistic conditions, as well as its behavior under feedback control. We also point to possible experimental and theoretical extensions of this work.

## 2. Experiments

In order to relate our modelling/computational results with the physics of the problem, it makes sense to include here a brief description of the apparatus used in Benziger et al. (2007a, 2007b) which we are here trying to model. As illustrated in Fig. 1, the cell consists of two compartments or flow channels, the anode and the cathode, between which a membrane–electrode assembly is sandwiched (two ETEK electrodes with carbon supported Pt catalyst and a Nafion[TM] 115 membrane). Flow channels (1.6 mm wide $\times$3.2 mm deep $\times$75 mm long) were machined out of polycarbonate. At the cathode the channel was lined with a split stainless steel electrode along the length of the channel. The anode was lined with six split segmented electrodes. The reactant gases are dry hydrogen and oxygen, respectively, with inlet flow rates $F_A$ and $F_C$ maintained with mass flow controllers. Two types of setups will be considered in this work: in the *co-current* mode, hydrogen and oxygen flow in parallel and follow the same direction (vertically, from top to bottom); in the *counter-current*
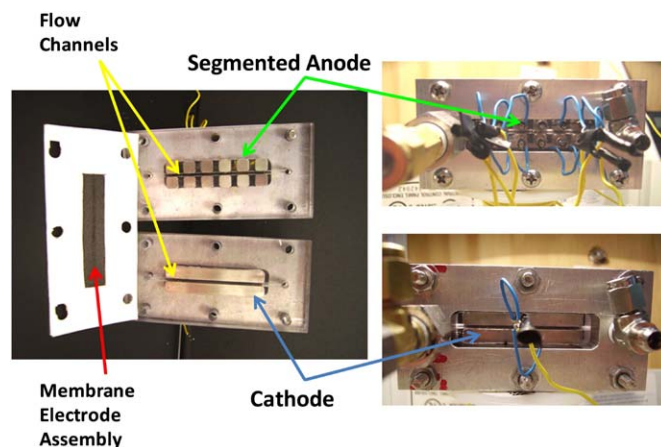


**Fig. 1.** A picture of the segmented anode fuel cell. The membrane electrode assembly consists of two ETEK electrodes with carbon supported Pt catalyst and a Nafion[TM] 115 membrane.

setup, the two reactants are flowing in anti-parallel directions: hydrogen flows up while oxygen flows down. These two configurations permit gravity to remove liquid water drops at the cathode; operation in horizontal configurations leads to very complex dynamical features, which were discussed in a previous publication but are beyond the scope of the present work (Kimball et al., 2008). The cell is kept at the desired operating temperature *T* through the use of two aluminium heating blocks.

The anode was broken in six equivalent segments separated by insulating spacers in order to record independently the current through each segment and the voltage drop across the external load resistor as a function of time (the lead wires from each anode segment being connected individually to a $0.1\,\Omega$ sensing resistor). The reactor was designed with the lateral separation between anode segments more than 10 times larger than the transverse separation between the anode and cathode, so that the transverse current is large compared to the lateral currents. Each of these segments has a total area of $0.5\,cm^2$. Note that the different segments are electrically connected *in parallel* with each other, as shown in the equivalent circuit (Fig. 2).

We will now turn to the simple physicochemical model we used to rationalize our results and compare its predictions with the actual experimental data.

## 3. The kinetic model

The basic mechanism of water formation in PEM fuel cells is now well understood. The $H_2$ molecules are adsorbed and dissociate at the anode, and the H atoms are subsequently oxidized to protons that are transferred to the PEM. At the level of the cathode, the $O_2$ molecules are adsorbed, they dissociate, and they subsequently react with the protons coming from the membrane to produce water. The electrons are transferred from the anode to the cathode through an external load resistance $R_L$. A voltage difference $V_L$ is generated between the anode and cathode, which drives a current *i* reflecting the rate of water production. The membrane plays a central role in such a device, since protons must be transferred through it in order for the reaction to take place. As was mentioned, we use Nafion[TM] membranes, which are partially substituted perfluorosulfonic acid ionomers. The transport of protons in such polymers can be greatly enhanced by the presence of absorbed water, ionizing the sulfonic groups and thus allowing for a proton hopping mechanism between fixed ions. Because of this, the membrane resistance strongly depends on the
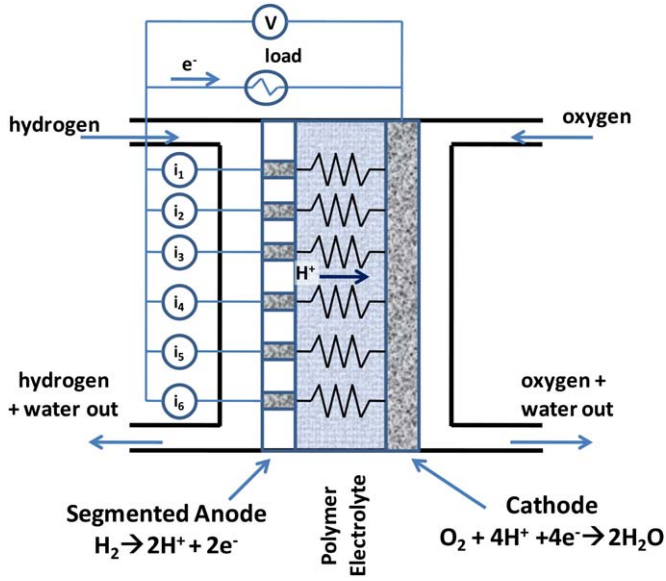
**Fig. 2.** Equivalent electrical circuit for the segmented anode fuel cell depicted in Fig. 1. Currents were followed in real time through the external sensing resistors and the total current was calculated by summing individual currents. The voltage across the load resistance was also recorded.

water activity in the membrane ($a_w$). The membrane resistance changes by six orders of magnitude as the water activity increases from 0 to 1, and is best fitted in our case by (Chia et al., 2007)

$$R_M(a_w) = 10^7 \exp(-14a_w^{0.2})\frac{l}{A} \text{ } (\Omega),$$ (1)

where $l$ and $A$ are the (local) membrane thickness and area. Under the operating conditions of interest, proton transport across the membrane is the rate limiting step in the formation of water.

Our main objective here is to build a relatively simple model in order to unravel the physicochemical basis of the observed phenomena. In order to do this, we focus on the balance of water produced in, and removed from, each of the compartments of the segmented fuel cell. Our main assumptions can be summarized as follows:

- The different segments of the cell are supposed to be locally homogeneous—the PEM fuel cell can thus be seen as a "tanks-in-series" reactor.
- All the intermediate chemical species, such as those adsorbed on the Platinum grains, are supposed to evolve on time scales which are much more rapid than the time scale of the observed phenomena, i.e. concentrations are quasi-stationary.
- Water absorption–desorption is fast and rapidly reaches equilibrium; the water vapor pressure and activity in the membrane are thus related by $p_w = p_w^0 a_w$, where $p_w^0$ is the water saturation vapor pressure at the temperature of operation. This assumption is probably the strongest in the model; water absorption can indeed be limited by polymer relaxation dynamics.
- We neglect formation of liquid water in the cell—this actually limits us to situations where the level of humidity inside the cell is not too high.
- The total pressure in each compartment remains constant (1 bar), in accordance with experimental observations.
- Possible mass-transport limitations of the gaseous species towards the catalyst are not considered.
- We use Nernst potentials, meaning we neglect overpotentials except for the ohmic potential drop—i.e. the rate limiting step is proton transport across the membrane.

- Concerning mass transport phenomena, we only consider gas convection in the flow channels and water diffusion occurring in the membrane due to the water activity gradient.

Taking this into account, the time evolution for the water activity in each compartment ($j$) is given by

$$\left[N_{SO_3}\frac{d\lambda(j)}{da_w(j)} + (V_A + V_C)\frac{p_w^0}{RT}\right]\dot{a}_w(j)$$

$$= \frac{i(j)}{2\mathcal{F}} + [F_A(j-1) + F_C(j-1)]p_w^0 a_w(j-1)$$

$$- [F_A(j) + F_C(j)]p_w^0 a_w(j) + k_m[a_w(j+1) + a_w(j-1) - 2a_w(j)]$$ (2)

in the co-current case and by

$$\left[N_{SO_3}\frac{d\lambda(j)}{da_w(j)} + (V_A + V_C)\frac{p_w^0}{RT}\right]\dot{a}_w(j)$$

$$= \frac{i(j)}{2\mathcal{F}} + F_A(j-1)p_w^0 a_w(j-1) + F_C(j+1)p_w^0 a_w(j+1)$$

$$- [F_A(j) + F_C(j)]p_w^0 a_w(j) + k_m[a_w(j+1) + a_w(j-1) - 2a_w(j)]$$ (3)

for counter-current setups. The segment number is given with respect to the anode inlet. In each case, the water vapor pressure is set to 0 at the level of the inlets, and $a_w(0) = a_w(7) = 0$. The left-hand sides in these equations correspond to the accumulation of water in the membrane and the gas channels. $N_{SO_3}$ is the total amount of sulfonates in the membrane delimited by each compartment. It can be evaluated noting that the density of Nafion$^{TM}$ is $\approx 2$ g/cm$^3$, so that for a 0.0125 cm thick membrane the area density is 25 mg/cm$^2$. With a local active area of 0.5 cm$^2$ and an equivalent weight of 1100 g/mol$_{SO_3^-}$, one gets that $N_{SO_3} \approx 1.13 \times 10^{-5}$ mol. If we take in addition into account the amount of polymer brushed on the catalyst, we finally get $\approx 1.2 \times 10^{-5}$ mol, which will be used throughout this paper. Note that $\lambda(j)$ is the water uptake (average number of water molecules per sulfonate). $V_A$ and $V_C$ stand for the constant volumes of the anode and cathode, respectively. The right hand sides contain the rate of water production, which is half of the local current divided by the Faraday constant, water exchange through convection in the gas phase ($F_A(j)$ and $F_C(j)$ are the local molar flow rates in the anode and cathode compartments) and water exchange by diffusion in the membrane. The $k_m$ is an effective mass transport coefficient which is the diffusivity of water in the membrane (considered here as constant) divided by the distance between compartments, multiplied by the cross sectional (constant) area of the membrane, as estimated in Chia et al. (2007). Note that our assumption of constant total pressure in the gas compartments imposes that $F_A(j) = F_A(j-1) - i(j)/4\mathcal{F}$ while $F_C(j) = F_C(0), \forall j$.

An expression for the current and $\lambda$ as functions of the water activities is necessary to close the above evolution equations. For Nafion$^{TM}$ 115 membranes, an empirical fit of $\lambda$ is available (Yang et al., 2004):

$$\lambda(j) = 14.9a_w(j) - 44.7a_w^2(j) + 70a_w^3(j) - 26.5a_w^4(j) - 0.446a_w^5(j).$$ (4)

Concerning the current, it is important a this stage to recall that the different segments are in fact electrically connected in parallel to each other. The local current is thus given by

$$i(j) = \frac{V(j) - R_L\sum_{k \neq j}j(k)}{R_M(j) + R_L} \text{ (A)},$$ (5)

where $V(j)$ is the voltage across the segment, $R_L$ is the load (external) resistance and $R_M(j)$ is the (local) membrane resistance depending on the (local) water activity, as given by Eq. (1).

**Table 1**
Numerical values of the constants and parameters introduced in the expression for the membrane resistance $R_M$ and in the model.

| Notation | Signification | Numerical value |
|---|---|---|
| $A$ | Local membrane area | $0.5\ cm^2$ |
| $k_m$ | Effective diffusion coefficient | $5 \times 10^{-7}\ mol/s^{-1}$ |
| $l$ | Membrane thickness | $0.0127\ cm$ |
| $N_{SO_3}$ | Number of moles of $SO_3^-$ | $1.2 \times 10^{-5}\ mol$ |
| $p_{tot}$ | Total pressure | $1\ bar$ |
| $V_A, V_C$ | Flow channel volumes (anode, cathode) | $3.33 \times 10^{-5}\ L$ |

As was mentioned, we consider simple Nernst potentials so that

$$V(j) = 1.23 + \frac{RT}{4\mathcal{F}} \ln \left[ \frac{p_{H_2}^2(j) p_{O_2}(j)}{p_{tot}^3 a_w^2(j)} \right] \ (V). \tag{6}$$

Note that we neglect here interfacial voltage drops and mass-transfer limitations, so that the currents predicted by the model will in general be higher than those reported in experiments, for similar parametric conditions. This last relation actually closes the kinetic equations, in view of our assumption of constant total pressure: $p_{H_2}(j) = p_{O_2}(j) = p_{tot} - p_w(j) = p_{tot} - p_w^0 a_w(j)$. The numerical values and units used for the different constants can be found in Table 1.

This system presents a strongly nonlinear response of the local water production rate with respect to the local water content, because the membrane resistance depends exponentially on the water activity. There is in fact a strong analogy to the positive feedback leading to ignition and spatiotemporal front propagation in exothermic chemical reactions, in which the heat produced enhances the reaction rate by raising the temperature. In our case, $H_2O$ enhances its own production by decreasing the membrane resistance, which in turn increases the current and hence the rate of water formation. It was recently demonstrated, through experiments and modelling, that water generated in a STR PEM fuel cell can "ignite" the current and that steady state multiplicity can be observed. The model hereby presented is in fact an extension of the one we developed for the STR cells. In the homogeneous limit ($a_w(j) = a_w$, $\lambda(j) = \lambda \forall j$), Eqs. (2) and (3) can be cast into the form

$$6 \left[ N_{SO_3} \frac{d\lambda}{da_w} + (V_A + V_C) \frac{p_w^0}{RT} \right] \dot{a}_w = \frac{i}{2\mathcal{F}} - [F_A + F_C] p_w^0 a_w,$$

where $i = \sum_j i(j)$, $F_C = F_C(0)$ and $F_A = F_A(0) - i/4\mathcal{F}$, and which is exactly the same as the one used in our investigations of STR cells (Benziger et al., 2004, 2005). This equivalent STR has a gas volume and membrane area which are six times larger than the differential elements in the segmented-anode model.

The experiments revealed mainly two types of dynamic features for the segmented PEM fuel cell described above: (i) multiple stable steady states with specific current profiles across the cell and (ii) nonlinear ignition/extinction phenomena accompanied by a wave-like propagation of the current along the cell. We will first turn to the steady state properties and see how the model can help understand their specificities.

## 4. Bifurcation diagrams and polarization curves

The stationary properties of the modelled segmented anode fuel cell were investigated using the AUTO-07p continuation package, the latest evolution from the AUTO software developed by Doedel (1981). Four operating parameters can be considered: the load resistance, the temperature and the hydrogen or oxygen inlet flows; we chose to present the steady state properties by considering two- and one-parameter diagrams for the different fuel cell configurations, along with the predictions of the well-stirred system.

As can be seen in the two-parameters diagrams (Fig. 3), the spatially extended systems obviously share common qualitative features with the STR limit. In particular there exists a region with multiple steady states which is delimited by critical values for the four different parameters. In this region of multiplicity, three states appear: one stable state corresponds to an inactive cell (almost zero current), and one to a reactive state with high current densities. These states have also been observed in experiments, as was reported earlier. The intermediate state is unstable (see for example one-parameter diagrams such as those in Fig. 4). A cusp signalling the disappearance of the bistable parametric region is often found within acceptable values of the manipulable parameters, except for the flows of reactants. The parameter region supporting bistability differs form one configuration to the other. As a rule, spatially extended systems typically display multistability at lower temperatures, load resistance or flow compared to the well-stirred system. Accordingly, the active state disappears "earlier" in the segmented anode model. This effect is even more pronounced in the case of co-current propagation of reactants. Running the cell as a plug flow-like reactor thus seems to make it more sensitive to drying conditions.

To understand the basic physical mechanism behind this effect, it is instructive to turn to the steady state spatial distribution of the current in the active state. The extinguished state is not plotted as it is always very close to zero. As shown in Fig. 5, the current is not distributed homogeneously throughout the cell, but presents a well-defined profile. In the co-current case, the last segments are always more active than those close to inlets, and the internal gradient of activity increases when increasing the $H_2$ inlet flow rate. For counter-current configurations, the current typically exhibits a maximum whose position is determined by the ratio of hydrogen and oxygen feed rates. It is important at this point to recall that: (i) high flows strongly affect the dynamics by quickly removing water from a segment, hence favoring the dry inactive states and (ii) the hydrogen flow rate changes from one segment to the other, decreasing with the distance from the hydrogen inlet since $F_A(j) = F_A(j-1) - i(j)/4\mathcal{F}$. In a sense, the segments close to the hydrogen inlet behave as if they were single STR cells exposed to rather high flows: for example, the first segment is subjected to a flow $F_A(1) = F_A(0) - i(1)/4\mathcal{F}$. The part of the cell located far from the hydrogen inlet feels a lower molar flow rate since, e.g. $F_A(6) = F_A(0) - \sum_j i(j)/4\mathcal{F}$: compared to the inlet flow rate, the flow in any compartment is reduced by the integral of the current up to this point. This natural tendency to have inactive compartments close to the $H_2$ inlet, and more active ones far from it creates a gradient in water activity. For counter-current operation, this gradient is reduced by diffusion of water in the membrane, and through the convective transport of water in the cathode gas phase, since $O_2$ flows against the water gradient created by the hydrogen flow. In the case of co-current flows, this gradient is exacerbated by the transport of gaseous water at the cathode, which tends to further dry out the first segments. The only counterbalancing process is then water diffusion, which given our numerical estimates is often not enough to mix the system and restore a more uniform water content throughout the cell. This difference between the two modes could explain why co-current operation leads to globally drier systems and tends to extinguish more easily. Despite these limitations, it should be noted that spatially extended self-humidified cells could in theory be operated at relatively high temperatures, if the flows and the load resistance are chosen with care. This tendency has also been observed in experiments (Hogarth and Benziger, 2006), but a
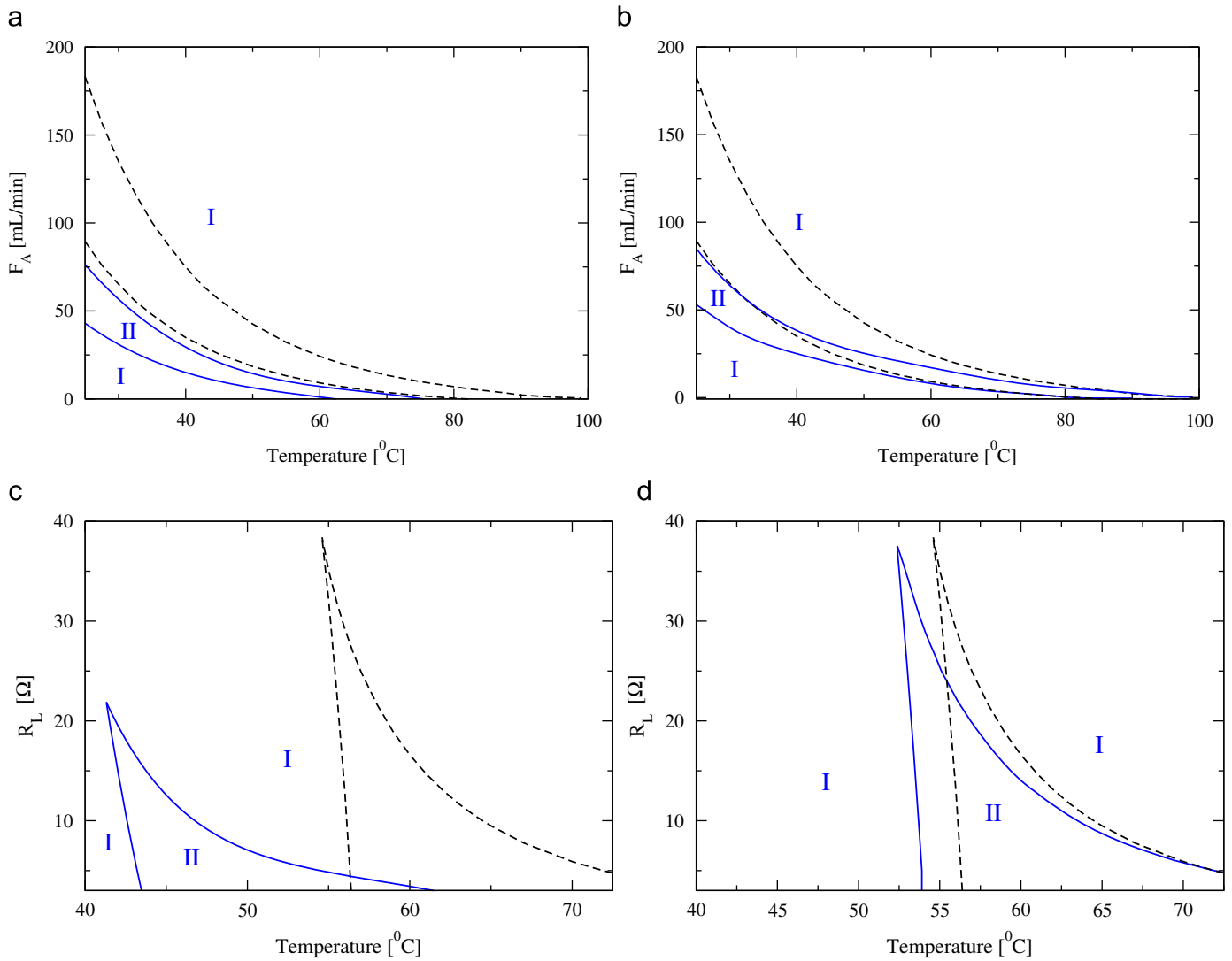
**Fig. 3.** (Color online) Two-parameter diagrams, plotting the boundaries between monostability (zones I) and multistability (zones II). (a and b) Plot the critical hydrogen flow as a function of temperature, for co-current and counter-current operations, respectively ($R_L = 5\,\Omega$, $F_C(0) = 6\,\text{mL/min}$). (c and d) Give the corresponding critical load resistance as a function of $T$ ($F_C(0) = 6\,\text{mL/min}$, $F_A(0) = 12\,\text{mL/min}$). The dashed lines are the results obtained for the homogeneous (STR) model.
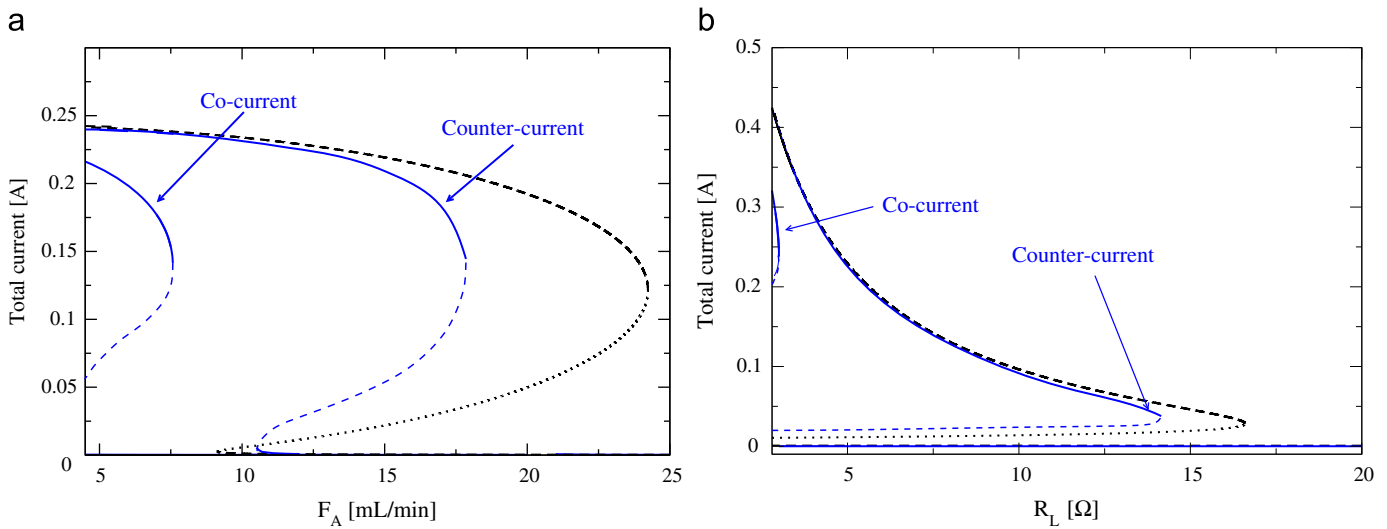


**Fig. 4.** One-parameter bifurcation diagrams showing the two stable states and the unstable state, for the different configurations, as a function of: (a) the hydrogen inlet flow rate ($R_L = 5\,\Omega$, $F_C(0) = 6\,\text{mL/min}$ and $T = 60\,^\circ\text{C}$) and (b) the load resistance ($F_A(0) = 12\,\text{mL/min}$, $F_C(0) = 6\,\text{mL/min}$ and $T = 60\,^\circ\text{C}$). Unstable states are denoted by dashed lines in the co-current and counter-current modes. The remaining curve represents the STR system, where the unstable state is pictured by a dotted curve.
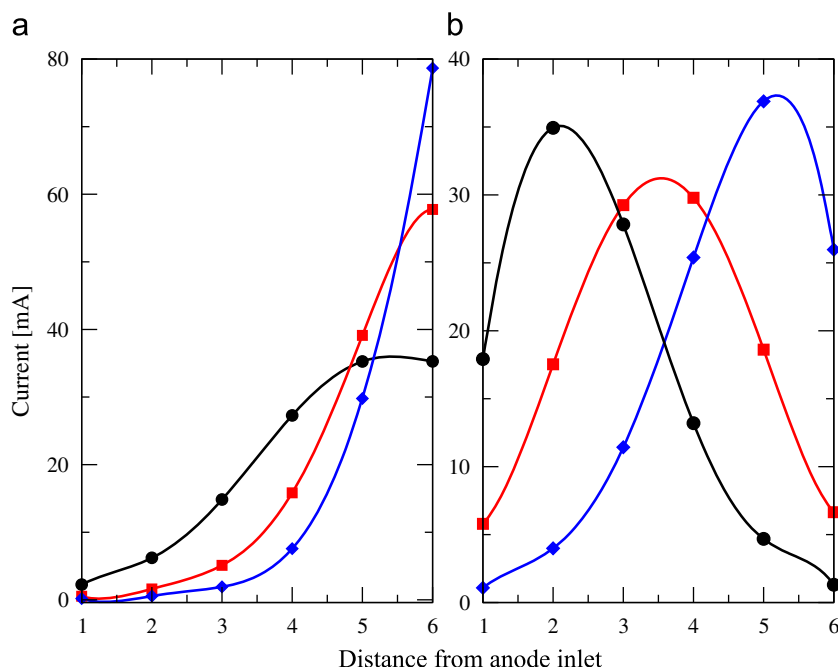
**Fig. 5.** Steady state current profile, as a function of the distance from the H$_2$ inlet for: (a) the co-current and (b) the counter-current configuration. In each case, $F_C(0) = 12$ mL/min; the circles (black), squares (red) and diamonds (blue), respectively, correspond to $F_A(0) = 6, 12$, and 18 mL/min. The smooth curves serve as a guide to the eye. The other parameters are the same as in Fig. 4a. (For interpretation of the references to color in this figure legend, the reader is referred to the web version of this article.)
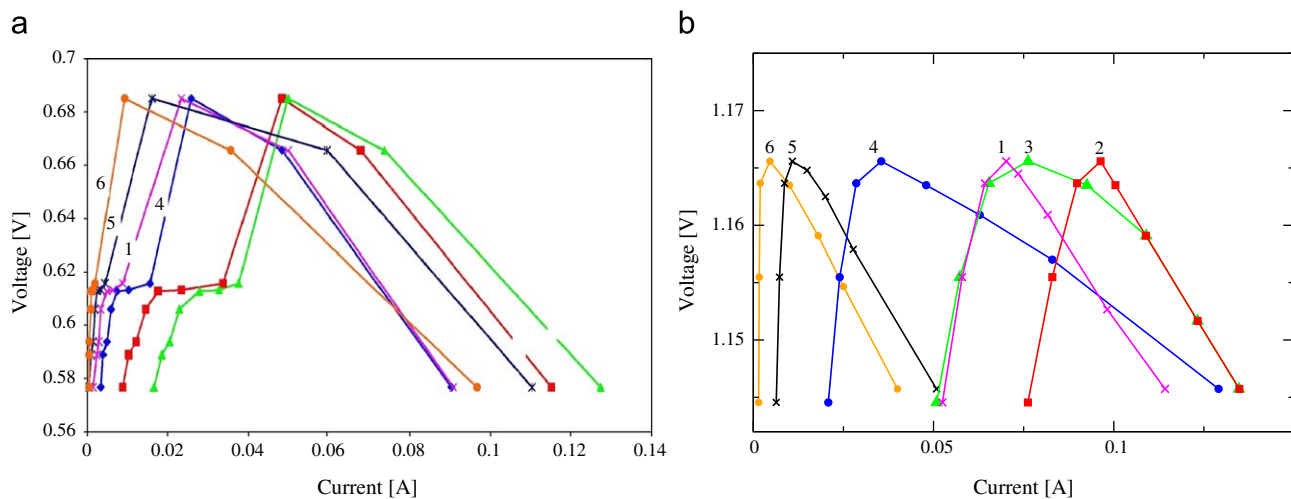


**Fig. 6.** (Color online) Experimental (a) and theoretical (b) polarization curves obtained in the counter-current mode. In the experiments, the originally ignited cell is run at 80 °C with $F_A(0) = 6$ mL/min, $F_C(0) = 3$ mL/min, and $R_L$ is varied from 2 to 20 Ω after letting the system relax for 2 h. In the simulations, the temperature, the flows and changes in the external load are identical but the system has to be relaxed for 1 h to obtain comparable curves. Note that in these figures, the segment numbers are counted from the cathode inlet, e.g. segment 6 is located next to the hydrogen inlet.

more systematic study (i.e. bifurcation diagrams) should be performed to better delimit the applicability of this type of cells to high temperatures.

The experimental investigations also revealed unexpected polarization ($i$–$V$) curves (Benziger et al., 2007a). These curves record the voltage drop across and current through the load resistance as the resistance is varied from 0 (short circuit–maximum current) to infinity (open circuit–zero current). At low current (high load resistance) an activation region is found, due to the need for electrons to overcome some activation barrier. For intermediate currents, an Ohmic region is observed where the polarization curve is typically linear with a slope equal to minus

the resistance. Finally for high currents (low load resistance), one finds a region corresponding to limitations in the transport of reactants toward the electrodes. The situation we observed experimentally for the self-humidified PEM fuel cell is, however, much more complex (see Fig. 6). Starting from its ignited state, the system was allowed to relax for 2 h at load resistances ranging between 2 and 20 Ω, with steps of 2 Ω. Note that our experimental setup allows for the measurement of the current flowing through each compartment of the cell, so that "local" polarization curves can be obtained, plotting $V_L$ as a function of $i(j)$. The resulting curves are strongly nonlinear. For low currents, the voltage is quite low and is increasing with the current until some critical value is

reached, after which the voltage starts decreasing. The effect has been observed for co-current and counter-current operations, but we only report on the latter in this work. Very similar results could be obtained when simulating the evolution Eq. (2) or (3) for a final time of 1 h (see Fig. 6b). It should be noted, however, that the voltage drop after the maximum is not as pronounced in our simulations as in the experiments. We believe the main reason behind this is our neglecting of flooding in the simple model we use here: at high currents, water created by the reaction can accumulate in the gas diffusion layer and hinder the transport of reactants to the electrodes, strongly reducing the current and voltage (Kimball et al., 2008; Weber and Newman, 2004). Another explanation could relate to the fact that we do not include activation overvoltage. Since overpotentials at the cathode can often be related to the presence of liquid water, these two contributions might actually be strongly intertwined. This idea is supported by the fact that much more realistic values are obtained using more sophisticated models where flooding is taken into account (Chia et al., 2007).

The reason behind this nonlinear response can be rationalized on the basis of our simple model. The voltage across the external load is given in our approach by $V_L = R_L i = V(j) - R_M(j)i(j)$, with $i = \sum_j i(j)$, since the different segments are connected in parallel with each other. The local cell voltage, $V(j)$, depends on the local water content $a_w(j)$ (and hence the current) but varies slightly as its dependence in this variable is logarithmic. The product $R_M(j)i(j)$ on the other hand strongly depends on the local current since the membrane resistance decreases exponentially with $a_w$ (which is high when the current is high). This contribution to the voltage across the load is thus large for low currents and for large currents (since it depends linearly on $i(j)$), and can present a minimum in between. This is the result of the variation of resistance on water activity, which is specific to the class of systems we study here (self-humidified cells). Cells operating at high humidity levels present a constant membrane resistance, so that the normal monotonically declining polarization curve is usually obtained. This idea can be confirmed

experimentally by obtaining *instantaneous* polarization curves, i.e. curves obtained by rapidly changing the external load. In that case, the classical linear behavior is again obtained since $R_M$ remains virtually constant during these "fast" measurements.

Finally, it should be noted that while the experimental and numerical simulations are run for apparently long times (several hours), the state which is reached in this way is not the "true" steady state, as can be easily verified using AUTO. By comparison with traditional numerical integration, it can be shown that the steady state is reached after 500–1000 h. Within the framework of the simple model we use here, the final voltage then increases as a function of the current until it reaches a plateau; i.e. the voltage drop for large currents is lost. This long relaxation time shows that the evolution of the cells should be analyzed with care in order to get a proper view of their behavior. We will thus now turn to their spatiotemporal dynamics.

## 5. Ignition and extinction phenomena

Experiments revealed that the ignition and extinction of the self-humidified cells are accompanied by characteristic pattern formation, in the sense that waves of current were seen propagating between the different segments. We detail the corresponding experimental and theoretical results in the next two subsections.

### 5.1. Ignition of the cell

To follow experimentally the development of currents during its startup, the cell was first pre-conditioned with a $20\,\Omega$ load at $60\,°C$ and flow rates of 3.5 mL/min $H_2$ at the anode and $O_2$ at the cathode for 8–12 h (more details can be found in Benziger et al., 2007a). The current in each segment was then $<1$ mA. Starting from this dry and inactive state, ignition could be triggered by injecting a small amount of water, or by drastically diminishing
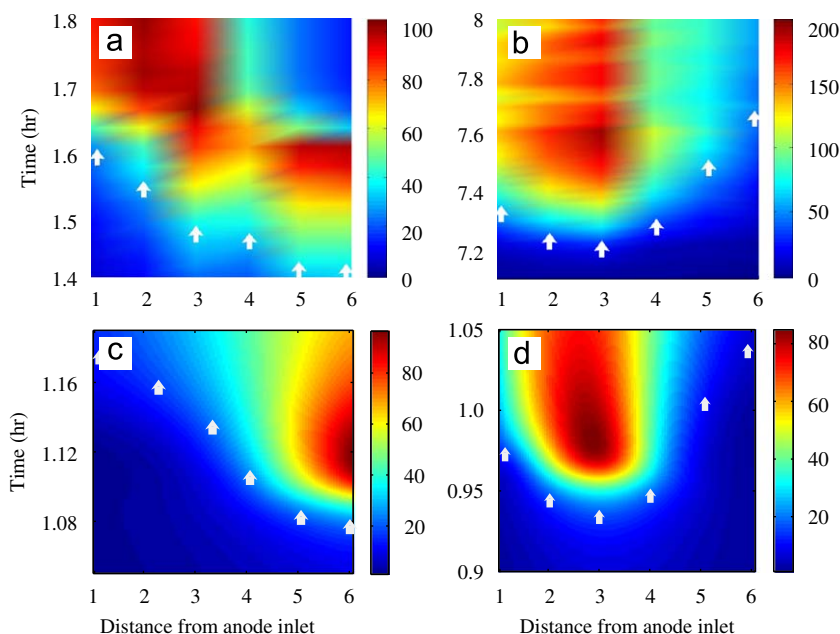


**Fig. 7.** Experimental and computed currents for co-current and counter-current flows in a segmented anode PEM fuel cell. The vertical axis is the time (in hours) and the horizontal axis is the segment number (counted from the anode inlet). The color scale is for current through each anode segment in mA—a horizontal smoothing procedure (Matlab spline function) has been applied for the sake of visibility: (a) experimental co-current; (b) experimental counter-current; (c) computed co-current; and (d) computed counter-current. In the experiments, the hydrogen and oxygen flow rates were 3 and 6 mL min$^{-1}$, the load resistance $0.5\,\Omega$ and the temperature was 298 K. For the simulations, $F_A$ and $F_C$ are, respectively, 3.5 and 6.5 mL/min, $R_L$ is $5\,\Omega$ and $T = 313$ K. The white arrows indicate the approximate ignition time for each segment. (For interpretation of the references to color in this figure legend, the reader is referred to the web version of this article.)

the temperature, the external load and/or the inlet flows. For the experiments displayed in Fig. 7, the temperature was for example reduced to 25 °C, and the load resistance reduced to 0.5 Ω, increasing the water production. This rather specific procedure points to the idea that the cell must: (i) be in a given region of parameter space and (ii) go "over" some critical state before ignition can take place, which is in line with the multistability we described in the previous section. The subsequent ignition is characterized by a long (several hours) transient stage where the current remains almost unchanged, followed by an abrupt change (15–20 min) leading the system toward an active state. Note that in the example depicted here, the current in the last segment decreases for long times in the co-current mode. This feature is only observed when liquid water was also seen to flow out of the cell; otherwise the steady state current increased monotonically from the inlets to the outlets.

The ignition does not take place homogeneously, but through the emergence of a "high current spot" (the analog of a hot spot for exothermal reactions) which subsequently propagates throughout the cell. Note that since high currents lead to large water production rates, this mechanism also corresponds to the nucleation and propagation of local wet spots. When operating in the co-current mode, the initial spot is always located at the end of the cell (i.e. far from the inlets) and then propagates towards the gas inlets (Fig. 7a). In the counter-current mode, the position of the first spot depends on the ratio of inlet flows, but is often found to be close to the center of the cell. The current activity then propagates outwards (Fig. 7b). As was noted before, the final steady state current consequently present a characteristic spatial profile. Simulations from our simple model lead to qualitatively comparable results (see Fig 7c and d). The location of the first wet spot is in particular reproduced quite accurately, as well as the "incubation time" of the transition phenomenon. We observe, however, that drier conditions must be considered in general in simulations to get current densities similar to those obtained in experiments. This can be traced back to the fact that our approach overestimates the cell potential, as was mentioned earlier. Also, the model is unable to reproduce the drop in current sometimes observed in the co-current mode, since it neglects the formation of liquid water which was observed in the experiments in that case. In consequence, the model typically offers a good description of the short time behavior. Note that since such a current drop is not found in the counter-current setup, our simple model actually describes quite well both the short- and the long-time behavior.
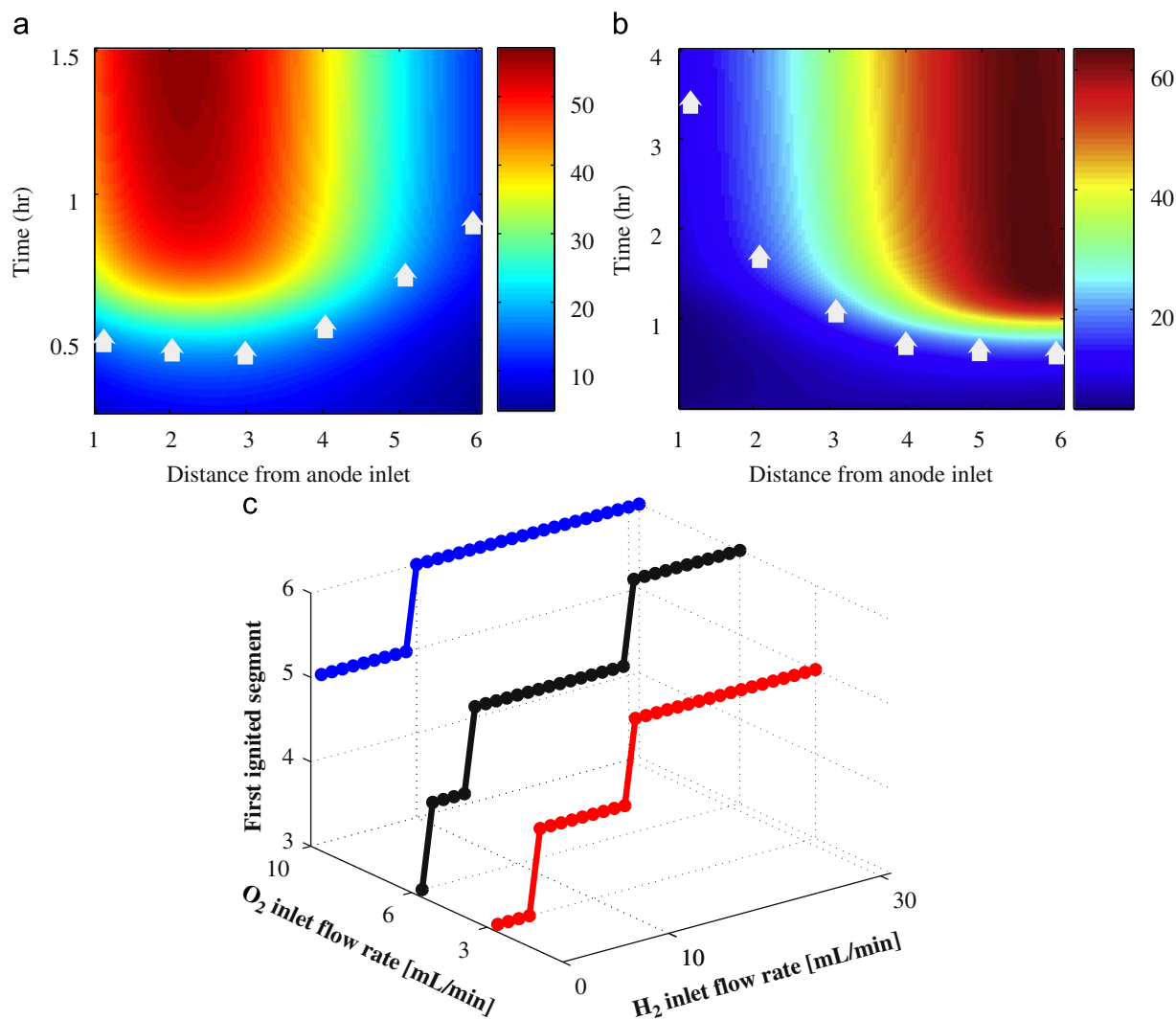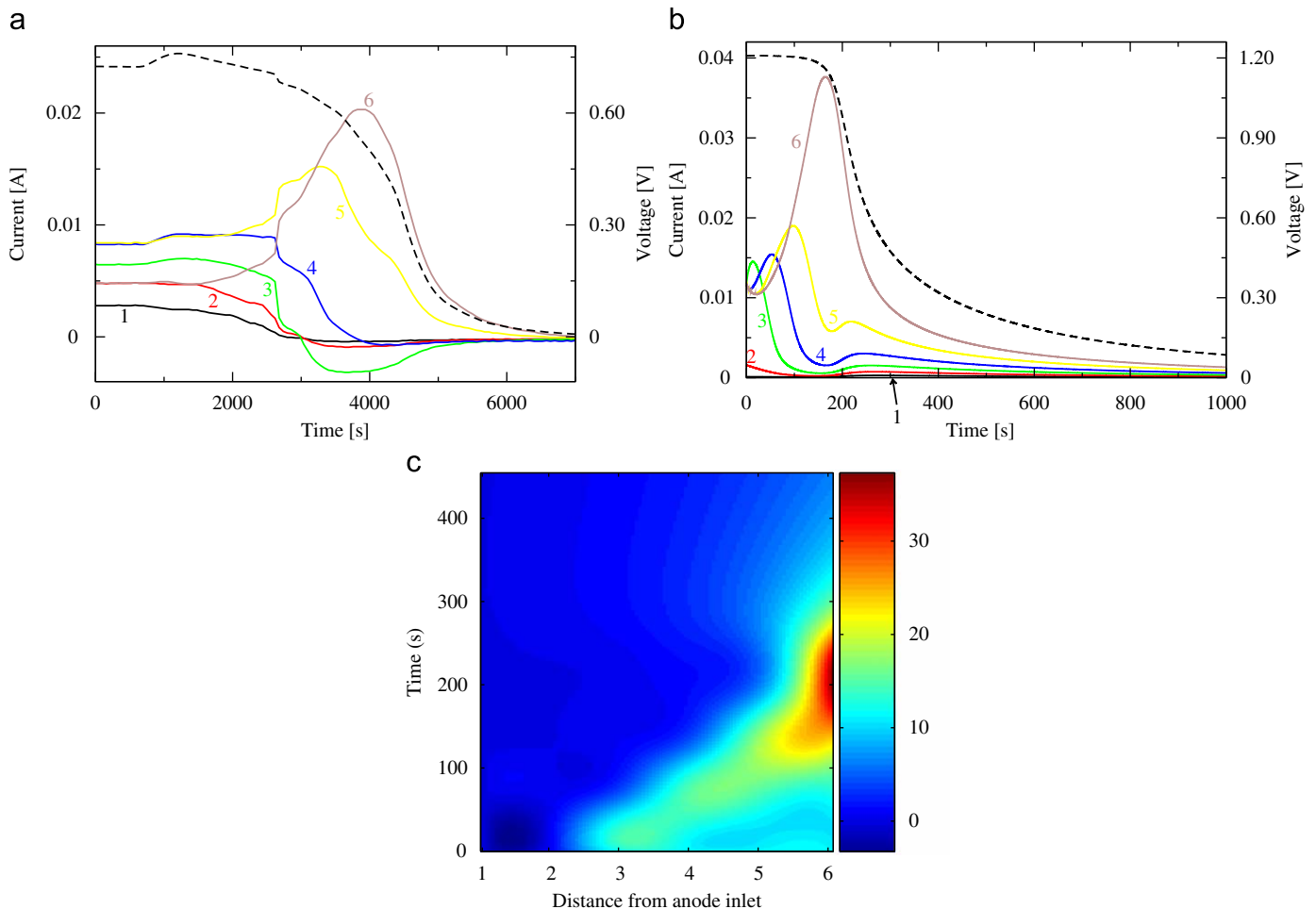


**Fig. 8.** (a, b) Are spatiotemporal plots of the currents (in mA), respectively, corresponding to $F_C(0) = 10$ mL/min and $F_A(0) = 3$ mL/min (ignition close to the center), and $F_C(0) = 3$ mL/min and $F_A(0) = 10$ mL/min (ignition close to the outlet). (c) Plots the localization of the first igniting segment for counter-current flows, as a function of the hydrogen inlet flow, for different values of $F_C(0)$: 3 mL/min (blue), 6 mL/min (black) and 10 mL/min (red). The temperature is 333 K and $R_L = 5$ Ω. (For interpretation of the references to color in this figure legend, the reader is referred to the web version of this article.)

Despite these limitations, the simplicity of the model allows for a physically intuitive explanation of the observed current propagation. The basic mechanism is very similar to the case of the STR fuel cell: water needs to build up to a level which is high enough to trigger its own catalytic production, i.e. high enough to enter the basin of attraction of the ignited state. The flow pattern, however, affects this simple picture of the ignition phenomenon. In the co-current case, water produced close to the gas inlets is rapidly convected away toward the outlets and can accumulate in the last segments. The rate of water production is thus typically higher there than in the rest of the cell. During the long "waiting" stage, the water activity there slowly increases, due to the competition between: (i) local autocatalytic production and vapor coming from the previous segments and (ii) water removal from the gas phase (convection) and from the membrane (diffusion toward the drier segments). When the local water content is sufficiently high in the last segment, it undergoes a rapid transition to the ignited state and the large amounts of $H_2O$ produced in this way can diffuse back (through the membrane) and "contaminate" the rest of the cell. A similar mechanism can be associated with the counter-current mode, but in this case water is convected from both sides of the cell, so that it accumulates preferentially near the center. A systematic study of the simulations reveals that the location of the first "wet spot" could be controlled by the ratio of inlet gas flows in the counter-

current case. The first wet point can be moved closer to the $O_2$ inlet when hydrogen comes in more rapidly (see Fig. 8). For high $F_A(0)/F_C(0)$ ratios, the situation actually becomes very similar to the co-current case we encountered before, with the first wet spot appearing in segment 6.

The simulations also show that the nonlinear characteristics of self-humidified PEMFCs can have very practical consequences for the cell utilization. For example, the time necessary to reach the ignited state strongly depends on the operating parameters, which vary crucially across different practical applications. Very long response times are observed when one tries to start up the cell close to the boundary of the multistable regime; this is to be expected, since bifurcation theory predicts a "slowing down" of the dynamics in such regions. Another important consequence of the limited bistability region is that the cell cannot be started at all when the parameters place the system outside the region of existence of the active state, i.e. the cell will remain indefinitely in the extinguished state. Finally, it is worth noting that certain currents cannot be reached by such cells because they actually correspond to unstable steady states. These effects all point to the idea that a good knowledge of the underlying bifurcation properties is essential for the efficient operation of fuel cells under steady state operation or with slowly varying parameters. Previous results also suggest that self-humidified PEM fuel cells could be operated efficiently at low temperatures (below 60 °C) by



**Fig. 9.** Experimental (a) and theoretical (b) extinction curves of a co-current cell showing the local currents and the voltage across the load (dashed line) as a function of time. (c) Is a spatiotemporal plot of the current extracted from simulations. In both the experiments and simulations, the cell was first run co-current at 80 °C with flow rates of 12 mL/min $H_2$ and 6 mL/min $O_2$ and a load resistance of 0.5 Ω for a few hours. The load resistance was then increased to 20 Ω (in $t = 0$).

adjusting flow rates (Büchi and Srinivasan, 1997). Our experiments and model show that the temperature limit is not fixed and the cell could be run in more drastic conditions; the knowledge of the autonomous bifurcation diagram might then assist in rationalizing feedback loops dynamics.

## 5.2. Extinction of the cell

The extinction of the cell can be observed experimentally when one increases the temperature, the load resistance or the inlet flow rates, which all lead to a decrease in the rate of water production: if the rate of water convection exceeds the rate of production, the membrane dries out and the cell extinguishes. The experiments again show that the currents propagate in the cell following a very characteristic pattern. For example, as detailed in Benziger et al. (2007a), an active co-current cell can be switched off by suddenly increasing the load resistance at relatively high temperatures (see also Fig. 9a). The change in the external load actually first results in a waiting period of about half an hour during which the currents remain more or less unchanged. Then a decrease of the current in the first segments (those close to the $H_2$ inlet) is observed while an initial increase, followed by a slow relaxation of the current, is seen in the last segments. The voltage across the load resistor and the total current follow a simple monotonous decrease. These features are also found in simulations (see Fig. 9b), but with the noticeable difference that the model does not reproduce the waiting time observed in experiments before the currents begin to change.

The model, however, allows once again for a simple explanation of the observed propagation pattern, in particular the transient increase in current. Increasing $R_L$ obviously affects all the segments simultaneously. The first segments are initially in a state of very moderate activity (remember the stationary current profile is inhomogeneous) and thus rapidly switch to the (dry) low current state, freeing some water in the gas phase. We observe in our simulations that the water released in this way is rapidly convected towards the segments located further from the inlet, which increases the water activity of these segments and induces a transient increase of current. The resulting "current wave" is especially apparent in the spatiotemporal plots, as can be seen in Fig. 9c. This wave reaches the last segment, where water tends to accumulate. The water then slowly evacuates by convection to the outlet and by diffusion from segment 6 to segment 5, and so forth, so that the current slowly extinguishes in the last segment. The back diffusion of water can actually even induce a second transient increase of current in some of the segments. The wet spots finally vanish when the excess water has been evacuated by convection to the exterior of the cell, and the cell then globally, slowly, extinguishes. The counter-current mode does not reveal any new phenomenon, in experiments as well as in the simulations. Again, the wettest (hence generally central) compartments first undergo an increase of activity, due to water vapor being pushed from both inlets to the interior of the cell, and then extinguish by giving water to the neighboring segments. This phenomenon reflects itself in a transient and small gain in activity for the drier parts of the cell which is coherent with the simple physical picture we discussed in the case of co-current ignition.

## 6. Conclusions

Experiments performed earlier on a simplified, self-humidified PEM fuel cell (Benziger et al., 2007a, 2007b) revealed intrinsically nonlinear behaviors during the startup and the extinction of the cells. During these transients, as well as at the steady state, a characteristic spatial distribution of the current was observed, whose properties are controlled by operating parameters (temperature, flow of reactants and external load). These specificities strongly affect the performance of the cell, including for example the time necessary for ignition/extinction and the total current delivered to the load.

We here performed a detailed parametric study of the semi-quantitative, one-variable tanks-in-series model we developed to understand the basic mechanism behind the above mentioned phenomena (Benziger et al., 2007a). The model revealed that the production, the redistribution and the removal of water actually play the central role. During ignition, water builds up at some locations allowing for a *local* ignition of the cell current due to a strong, water-induced *local* reduction of the membrane resistance. The position of this "wet spot" depends on a subtle balance between the inlet flows of $H_2$ and $O_2$. When the reactants go counter-current, they "meet" and react close to the center of the cell where the spot is observed. If they flow in the same direction, water tends to accumulate close to the cell outlet because water formed by the reaction is pushed there by convection of the water vapor.

This local ignition in turn induces the production of even more water, since the rate of $H_2O$ formation is directly proportional to the current - in other words water production is autocatalytic. This situation is very close to what was observed and modelled in the case of small, STR self-humidified PEM fuel cells, except that locally ignited segments of the cell are now in contact with other, drier segments. The wet spot created in this way can thus subsequently propagate throughout the cell by convection in the gas phase and/or diffusion in the membrane, thereby inducing a "current wave". The steady state current reached in this way is itself generally not homogeneous but is higher where the membrane is wetter and lower where it is drier; the global current is always lower than what it would be if water were homogeneously distributed. The model shows that this profile of water activity is also a function of the different operating parameters. During extinction, water is typically rapidly convected away from the inlets and tends to concentrate at some position before being evacuated. In consequence, some parts of the cell first feel an increase of current before the extinction takes place.

The different experimental features we observed can thus all be rationalized in terms of water management in the PEM fuel cells. One of the most important conclusions in our opinion is that inhomogeneous current profiles can develop which lead to lower than expected currents being delivered to the load. Such problems could be solved by selecting membranes where water could rapidly diffuse to restore a more homogeneous water content, and hence current profile. It should be emphasized, however, that the model hereby studied does not take into account all the complexity of water-related dynamics. Recent experiments showed that flooding can occur at the level of the gas diffusion layer, hindering gas transport towards the electrodes and hence the current produced by the cell (Kimball et al., 2008). Slugs and drops were also observed moving through the cell and are believed to be at the origin of current oscillations found when cells are run horizontally. These effects add to the complexity of the problem of water management in PEM fuel cells, which is definitely a central issue.

Problems could also arise that are related to the intrinsically nonlinear character of the cell dynamics. We observed for example extremely long waiting time for ignition or transient increases of current during extinction in some cases. The existence of "forbidden" currents, i.e. currents corresponding to intrinsically unstable states that cannot be reached, is of course also an issue. These problems could reveal even more difficult to deal with than that of water management: the nonlinear dynamics of the cells is

intimately related to the presence of polymer electrolytes themselves. As soon as the membrane resistivity decreases with increasing water content, an autocatalytic loop is present and can induce nonlinear behaviors. One possibility to avoid such undesired dynamics would be to completely rethink the design of the fuel cell and use membranes or other types of electrolytes with very different conductivity properties. Another, less demanding approach would be to implement feedback loops using one of the manipulable parameters in order to accelerate the intrinsic dynamics or to stabilize/control the current. An interesting question would then be to determine the level of controllability of the self-humidified PEM fuel cells spatiotemporal dynamics, when using global feedbacks such as the reactants inlet flow rates or additional resistances or transformers. This problem should actually form the basis of a future publication.

## Acknowledgments

## References

Benziger, J.B., et al., 2004. A.I.Ch.E. J. 50, 1889.
Benziger, J.B., et al., 2005. Chem. Eng. Sci. 60, 1743.
Benziger, J.B., Chia, E.J., JE, E., Kimball, E., Kevrekidis, I.G., 2007a. J. Electrochem. Soc. 154, B835.
Benziger, J.B., Chia, E.S., De Decker, Y., Kevrekidis, I.G., 2007b. J. Phys. Chem. C 111, 2330.
Büchi, F.N., Srinivasan, S., 1997. J. Electrochem. Soc. 144, 2767.
Chia, E.J., Benziger, J.B., Kevrekidis, I.G., 2004. A.I.Ch.E. J. 50, 2320.
Chia, E.J., Benziger, J.B., Kevrekidis, I.G., 2007. A.I.Ch.E. J. 52, 3902.
Doedel, , 1981. A Program for the Automatic Bifurcation Analysis of Autonomous Systems. Paper presented at Proceedings of the 10th Manitoba Conference on Numerical Mathematics and Computation, Winnipeg.
Fronk, M., 2005. Fuel cell vehicle commercialisation. In: Ninth Grove Fuel Cell Symposium, London, UK, 4–6 October. Elsevier, London, UK.
Grötsch, M., Hanke-Rauschenbach, R., Mangold, M., 2008. J. Fuel Cell Sci. Technol. 5, 021001.
Hanke-Rauschenbach, R., Mangold, M., Sundmacher, K., 2008. J. Electrochem. Soc. 155 (2), B97.
Hogarth, W.H.J., Benziger, J.B., 2006. J. Power Sources 159, 968.
Kimball, E., Whitaker, T., Kevrekidis, Y.G., Benziger, J.B., 2008. A.I.Ch.E. J. 54, 1313.
Luss, D., 1997. Ind. Eng. Chem. Res. 36, 2931.
Martin, A., 2005. What we have learned from vehicle demonstration programs? In: Ninth Grove Fuel Cell Symposium, London, UK, 4–6 October. Elsevier, London, UK.
Marwaha, B., Luss, D., 2003. Chem. Eng. Sci. 58, 733.
Marwaha, B., Sundarram, S., Luss, D., 2004. Chem. Eng. Sci. 59, 5569.
Moxley, J.M., Tulyani, S., Benziger, J.B., 2003. Chem. Eng. Sci. 58, 4705.
Nazarov, I., Promislow, K., 2006. Chem. Eng. Sci. 61, 3198.
Weber, A.Z., Newman, J., 2004. Chem. Rev. 104 (10), 4679.
Yang, C., et al., 2004. J. Membr. Sci. 237, 145.